Measuring radiofrequency field-induced temperature variations in brain MRI exams with motion compensated MR thermometry and field monitoring

Caroline Le Ster[1], Franck Mauconduit[1], Christian Mirkes[2], Alexandre Vignaud[1], Nicolas Boulant[1]*

[1]Université Paris-Saclay, CEA, CNRS, BAOBAB, NeuroSpin, Gif-sur-Yvette, France

[2]Skope MRT, Zurich, Switzerland

*Corresponding author: Nicolas Boulant, Université Paris-Saclay, CEA, CNRS, BAOBAB, NeuroSpin, Gif-sur-Yvette, France. E-mail address: nicolas.boulant@cea.fr

Running title: RF-induced temperature changes in brain MRI exams

Key words: MR thermometry, field monitoring, motion compensation, RF safety

Word count: ~5134

Abstract

Purpose: An MR thermometry method with motion and field fluctuation compensation is proposed to measure non-invasively sub-degree brain temperature variations occurring through RF power deposition during MR exams.

Methods: MR thermometry at 7T with a multi-slice EPI sequence and concurrent field monitoring was first tested in vitro to assess accuracy in the presence of external field perturbations, an optical probe being used for ground truth. In vivo, this strategy was complemented by a motion compensation scheme based on a dictionary pre-scan, as reported in some previous work, and was adapted to the human brain. Precision reached with this scheme was assessed on 8 volunteers with a 5 min-long low SAR scan. Finally, temperature rise in the brain was measured twice on the same volunteers and with the same strategy, this time by employing a 20-min scan at the maximum SAR delivered with a commercial volume head coil.

Results: In vitro, the RMS error between optical probe and MRT measurements was 0.02 °C with field sensors correction. In vivo, the low SAR scan returned a precision in temperature change measurement with field monitoring and motion compensation of 0.05 °C. The 20-min maximum SAR scan returned a temperature rise throughout the inner-brain in the range of 0-0.2 °C. Brain periphery remained too sensitive with respect to motion to lead to equally conclusive results.

Conclusion: Sub-degree temperature rise in the inner human brain was characterized experimentally throughout RF exposure. Potential applications include improvement of human thermal models and revision of safety margins.

Key words: MR thermometry, field monitoring, motion compensation, RF safety

Introduction

During an MR exam, the radiofrequency (RF) field transmitted by the coil deposits energy in biological tissues. At high field (≥ 3T), because of the relatively short wavelength of the RF field, this interaction results in non-uniform heating of these tissues that depends on the spatial distribution of the energy deposition, heat diffusion as well as spatially-dependent heat dissipation. The brain is a heat producer organ for which temperature is tightly controlled through homeostasis. It is very sensitive to heat stress: when brain temperature increases by only a few degrees, its function can be altered (1–3). Physiologic intra-cerebral and temporal thermal fluctuations have yet been reported, with for instance the presence of thermal gradients higher than 0.5°C between the centre of the brain and its periphery (4–6). These studies are however sparse on healthy human brains (7). According to the International Electrotechnical Commission (IEC) standards released in 2015 (8), absolute temperature during the entire MR exam must remain below 39 °C in the brain and temperature rise in the eyes must not exceed 1 °C. Although non-invasive in-vivo temperature measurement methods exist, it is currently not possible to measure in real-time the temperature of a scanned tissue with sub-degree precision, and thus to supervise the MR exam with a temperature control, because of the lack of sensitivity and/or accuracy of these methods. Only thermal ablative therapy MR exams, where temperature rises by 10 degrees or more, are performed under temperature supervision but at a coarser thermal resolution (9,10). Therefore, for simplicity, the control of energy deposition during routine exams is performed with the specific absorption rate (SAR), which is a measure of the RF power absorbed per unit of mass. In the normal mode of operation of the IEC, SAR limits on the head are set to 3.2 W/kg globally and 10 W/kg locally over 10 g of tissue for a sliding window of 6 min. A safety factor of 2 then is typically added by scanner and coil manufacturers. SAR distributions, especially SAR hotspots, can be predicted with electromagnetic field simulations followed by phantom validations (11). The temperature in the tissues can then be calculated with simulations using Pennes' bioheat equation (PBE) (12) or more complex thermal models (13,14). The use of SAR for MR exam supervision however presents some limits. On one hand, only a few in vivo studies were conducted in attempting to measure dynamically the temperature rise in the brain induced by RF power deposition. These studies, performed with invasive probes (15) and MR Thermometry (MRT) (16,17) on anaesthetised animals (thus impaired thermoregulation (18)), failed to validate PBE with the tissue property values available in the literature. Another limit of SAR supervision is the absence of physiological information in this metric which leads to weak correlation between local SAR and temperature (19), especially during long RF field exposures (20,21). On the other hand, SAR monitoring is generally considered a conservative approach of historically safe value. The price to pay for this potentially increased safety is a limitation of

energy deposition in MRI that can have direct impact on image quality and exam durations, especially at high magnetic fields. More relevant MR exam supervision with thermal information could thus increase reliability of RF safety and provide more freedom in protocols by adjusting repetition times, flip angles, pulse excitation trains, pulse bandwidths etc... The knowledge of the temporal dynamics of temperature variations induced by different scenarios of RF energy deposition could furthermore turn very valuable to characterize PBE model parameters. It could also have consequences on the mobile phone industry where, for the same reasons as for MRI, SAR remains the norm.

Several MR thermometry (MRT) methods have been developed to monitor non-invasively in-vivo temperature variations (22). Among them, the proton resonance frequency shift (PRFS) and the spectroscopy methods have proved sensitive enough to map sub-degree temperature variations in the human brain (17,23). The PRFS method (24), which relies on the change of the water-bound fraction with temperature, is reputed the most accurate MRT strategy available to measure small temperature variations with a good spatiotemporal resolution (10,25). Reaching sub-degree precision for the measurement of temperature rise in the brain with PRFS however remains challenging: at 7T, a temperature rise of 1 °C decreases the frequency only by 3 Hz compared to 300 MHz (i.e. -0.01 ppm/°C) (26). This shift can thus easily be hindered by other sources of field variation that can be significantly higher. In the brain, they originate from both external sources (B_0 field drift, breathing, cardiac pulsation) and internal sources caused by head motion (27). The effect of external sources of field variation on the phase image can be estimated and corrected for with field monitoring (28). To compensate for internal sources of field variation during an MRT scan, a motion compensation methodology was recently proposed, where the effect of head motion on the phase was estimated from a dictionary pre-scan (17). In that study, the technique was tested at 7T on an anaesthetised macaque with a 2D-GRE PRFS sequence acquired with 3 orthogonal slices to estimate motion in every direction from magnitude images, which was found to be critical despite anaesthesia. For a 20-minute scan with RF exposure set at the maximal SAR allowed by the scanner, this methodology returned a slow temperature rise reaching ~0.7°C in the centre of the macaque brain. The anatomy and physiology of the macaque, as well as the use of anaesthetic agents (18) however make these results difficult to extrapolate to human routine scans.

Models predict peak temperature rise on the order of 0.5 °C for head volume coils in the brain when exposed at maximal SAR (19,29). It is clear also that without heat dissipation, current SAR limits would yield significant temperature changes. The aim of the current study was thus to dynamically measure temperature changes in the human brain exposed to RF power deposition during an MR exam at 7T. To reach the necessary sub-degree precision with a

good spatiotemporal resolution, the temperature rise was measured using the PRFS method with retrospective field sensor correction to the second order of the spherical harmonics decomposition, along with a motion compensation step. Accurate motion tracking was ensured through a fast and full-brain coverage with a multi-slice EPI sequence using a volume TR of 1.2 s. This sequence was run continuously during several minutes in concert with strong RF power deposition. The temperature change was measured voxel-wise from the phase image for each time frame of the temporal series, thereby allowing a follow up of brain temperature variations throughout the scan. Two SAR regimes were explored with this methodology. First, the sequence was played during 5 minutes in a low SAR regime, i.e. the SAR resulting from the monitoring sequence excitation pulses, to quantify temperature stability or precision. In this regime, the SAR was less than 10% of the maximal level allowed by the scanner in its normal mode of operation. Within the second SAR regime explored, the MRT sequence was 21 minutes long and was played at maximal SAR during the last 20 minutes of the scan by means of an additional high-energy pulse emitted at 100 kHz offset frequency. Measurements were first performed on a phantom to assess the accuracy of the field sensor correction method in a motionless scenario, and then in vivo on n=8 healthy subjects.

Methods

MR Thermometry experiments

MR Thermometry experiments were performed with the proton resonant frequency shift (PRFS) method (24), where temperature change at time t and position $\vec{r}$ ($\Delta T(\vec{r},t)$ in °C) is computed as:

$$\Delta T(\vec{r},t) = \frac{\Delta\varphi(\vec{r},t)}{2\pi\nu\alpha TE}$$

Where $\Delta\varphi(\vec{r},t)$ is the phase difference (rad), ν the Larmor frequency (Hz), α the frequency shift per degree Celsius (-0.01 ppm/°C (26)) and TE the sequence echo time (s). Given its low sensitivity, the PRFS method benefits from increased magnetic fields.

Field sensors correction

When going to higher magnetic fields, the phase becomes more affected by external sources of field disturbance such as B_0 field drift, shim heating, breathing, cardiac pulsation and limb motion. A previous MRT study performed with a 2D-GRE sequence on the brain of an anaesthetised macaque showed the benefit of including correction of the magnetic field perturbations up to the first order of the spherical harmonic decomposition as measured by 16 magnetic field sensors placed on the receive part of the RF coil for PRFS temperature

measurements (17). Such a correction was furthermore needed in the current study since the EPI sequence is especially sensitive to off-resonance effects accumulated through the EPI train. A Skope (Skope MRT, Zurich, Switzerland) Clip-on field Camera was thus used to monitor and retrospectively correct for field fluctuations related to scanner instabilities and physiology up to the second order of the spherical harmonics decomposition. Within this setup, the probes were excited synchronously to the scanner acquisition at fluorine frequency and the signal received by the probes was used to perform a spatial field expansion on a full second-order spherical harmonics basis. This field sensors correction alone was verified in vitro in the presence of external field fluctuations by comparing the MRT corrected results with an optical probe measurement at one spatial location.

Motion compensation

The PRFS method consists in measuring brain temperature variations voxel-wise from a phase difference by subtracting a reference value measured before heating (24). This method thus is very sensitive to motion (27) caused e.g. by slow muscle relaxation, swallowing, cardiac pulsation and breathing, especially at high field. Numerical simulations performed in a previous study have shown the great sensitivity of phase versus motion, especially for rotations around the left-right axis, with a head rotation of 1° resulting in up to 10 Hz frequency shifts in the most sensitive brain regions (17). Motion-induced field disturbances caused by sources located inside the head (air cavities) are not well captured by the field sensors, which assume external and smooth fluctuations decomposable into low-order spherical harmonics (28). In the current study, given that scans ran continuously during 20 minutes, the phase of images reconstructed with the field sensor correction thus was still corrupted by head motion. A method was recently introduced to compensate for the effect of motion on the phase using a dictionary pre-scan (17). This method makes use of both the phase and the magnitude of the MRT images: during the dictionary pre-scan, the temperature is assumed to be constant (low SAR scan) so that phase variations are assumed to originate solely from head rotations and translations, that are estimated from the realignment of the magnitude images. For each voxel of the volume reconstructed from the 2D mutlislice acquisition, the influence of motion parameters on the phase can thus be estimated with a linear regression corrected for the voxel mean signal ($\beta(\vec{r}) = R_{dict}^{-1}\varphi_{dict}(\vec{r})$, where β is a coefficient vector describing the influence of motion on the phase, R_{dict} a matrix composed of the estimated motion regression parameters and φ_{dict} the measured phase in the voxel). The β coefficients estimated from the dictionary pre-scan were then applied to the thermometry scans to compensate for motion ($\varphi_{MRT\ scan,denoised}(\vec{r}) = \varphi_{MRT\ scan}(\vec{r}) - R_{MRT\ scan}\beta(\vec{r})$). When introduced, this method was validated on an anaesthetised macaque scanned with a 2D-GRE sequence that was acquired with 3 orthogonal slices. To apply this methodology in the current study for human scanning, it

needed to be modified to account for the higher encountered motion amplitudes. The acquisition strategy chosen here thus was a multi-slice EPI sequence with full-brain coverage. The latter allowed better motion estimation, while the EPI acquisition scheme allowed increased temporal resolution and better motion tracking.

Correction for background gradients

In MRI, the phase evolves with: $\gamma B_0 TE \times G/(G + G')$, where G is the effective gradient applied in the phase encoding direction in the EPI sequence and G' = ∇B_0 is the local background field spatial derivative in the same direction (30). In GRE sequences, the readout bandwidth can be such that G>>G' so that G/(G+G') ~ 1, whereas in EPI sequences the effective gradient is much lower in the phase encode direction (G~1e4 Hz/m in the current study). At high magnetic field, in areas with strong ∇B_0 such as air cavity interfaces, G and G' can be on the same order. The coefficient G/(G+G') was thus computed voxel-wise and corrected for by using measured B_0 maps.

MR imaging

This study was approved by the local Institutional Review Board (Comité de protection des personnes Sud Méditerranée, approval number 2018-A01761-54) and the volunteers provided informed written consent. Acquisitions were performed on n=8 healthy volunteers (27±7 years, 3 females/5 males, BMI 22±3 kg/m²) on a Magnetom 7T scanner (Siemens Healthineers, Erlangen, Germany) equipped with the Nova 1Tx-32Rx head coil (Nova Medical, Wilmington, MA, USA). For each volunteer, an automatic second order shim was performed prior to the imaging scans that consisted in an anatomical sequence, a reference scan (used for B_0 mapping and sensitivity profile estimation), and four MRT scans (a 5-minute dictionary pre-scan, a 5-minute stability scan acquired at low SAR and two 21-minute scans acquired at maximal SAR). The anatomical sequence was an MPRAGE with TR/TE/TI 3070/2.8/1100 ms, flip angle 9°, 1 mm isotropic resolution, 160 sagittal slices, FOV 256 mm, and parallel imaging with GRAPPA (R = 2), resulting in an acquisition time of 6:41 min. Reference scans were performed with a 2D-GRE sequence that included 20 interleaved sagittal slices of 5 mm thickness, 4 echoes and TR 1200 ms, TE1/TE2/TE3/TE4 2.67/3.41/4.15/4.89 ms, 3×3 mm² in plane resolution, FOV 192 mm, flip angle 4°, A>>P phase encoding and pixel bandwidth 2000 Hz/Px. The multi-slice EPI MRT scans were performed with the same orientation, resolution, volume TR, phase encoding direction and bandwidth as the reference scans. The sagittal orientation was chosen to allow a better estimate of motion around the Left-Right axis, which has been found the most critical for motion-induced frequency shifts (17). Other parameters were: slice TR 60 ms, TE 20 ms, excitation pulse flip angle 30°. A rectangular heating pulse of 3.6 ms was added in the sequence prior to the excitation pulse (31) to reach the maximal SAR.

To prevent spin excitation, this high-energy pulse had an offset of 100 kHz from the water resonance frequency. This heating pulse was disabled for the dictionary and stability scans. For the heating scans, the first minute of the scan was played at low SAR (i.e. disabled heating pulse) and at maximal SAR during the following 20 minutes (i.e. the heating pulse flip angle was adjusted to reach the maximal SAR level allowed by the scanner in its normal mode of operation). Reaching up to 12 W at the coil plug, for a 5 kg head thus leads to 2.4 W/kg for head-average SAR if all power is absorbed by the tissues.

A field sensors setup, composed of 16 ^{19}F NMR field probes positioned on the receive part of the RF coil and of a spectrometer, was used to record the magnetic field fluctuations concurrently with the image acquisition every 300 ms. The data of the field probes was used to perform a spatial field expansion on a full second-order spherical harmonics basis (ie, k_0, k_x, k_y, k_z, and 5 additional terms). The skipped k-space lines that could not be monitored due to the short TR of the multi-slice EPI scan were interpolated. Retrospective image reconstruction with field sensor (FS) correction was then carried out using the skope-i software (version 2021a). In a first step, B_0 maps and coil sensitivity profiles were estimated from the reference scan. In a second step, these B_0 maps were used to reconstruct images of the individual channels of the MRT scans using actual trajectories recorded by the field sensors with additional field fluctuation correction through an iterative conjugate gradient algorithm that included field coefficients of the spherical harmonics up to the second order (32). Complex combined images were finally reconstructed by multiplying the individual coil images by their respective sensitivity profiles and summing them.

Magnitude images of the MRT scans were registered with McFlirt (26) with 6 degrees of freedom (3 rotations and 3 translations), while phase images were compensated for motion, corrected for background gradients and used for temperature rise estimation. For all the MRT sequences, the reference phase value to compute temperature change was computed voxel-wise as the average over the first minute of the scan, where low SAR was applied. For each subject, the T1-weighted anatomical scan was then spatially normalised to the 1 mm brain template of the Montreal Neurological Institute (MNI 152), while temperature change maps projected to the anatomical scans were normalised to the 3 mm brain template. Temperature change maps of the individual subjects were spatially smoothed with a 9 mm kernel.

The FS corrected protocol was first tested on a 16-cm diameter spherical gel phantom composed of 1% agar and doped with a mixture of $CuSO_4$ (0.25 g/L) and NaCl (4 g/L). Reference temperature was monitored with a fibre optical probe (FISO technologies Inc., Quebec, Canada) inserted in the phantom for validation, and its position was determined using a proton-density weighted image. The α value of the phantom was determined using the same

procedure as described in (17). The ability of FS correction to accurately measure small temperature changes was assessed with a 25-minute MRT scan. The multi-slice EPI sequence was played at low SAR during the first five minutes of this scan and at maximal SAR during the next 20 minutes. The field was deliberately disturbed to mimic the effect of e.g. breathing or limb motion between minutes 10 and 15 of this scan by moving an additional phantom in the bore of the scanner. This secondary phantom was moved back and forth at the entrance of the scanner tunnel so that there was no mechanical interaction with the scanned phantom, i.e. only the magnetic field was disturbed. For illustration purposes, images of the multi-slice EPI sequence were reconstructed with the dedicated software both without any correction and with FS correction to the second order of the spherical harmonics decomposition.

In vivo, a 5-minute dictionary pre-scan was first acquired on every subject in order to determine the influence of head motion on the phase. The subjects were instructed to move their heads at random positions during this scan acquired at low SAR and images were reconstructed with field sensor correction. Head movements were of low amplitude and the subjects maintained each position for about 10 s to reach a steady state signal. For each time frame of the series, six motion parameters (3 translations and 3 rotations) were estimated from magnitude images and β parameters were estimated for every subject and every voxel. These estimates were then used to compensate for motion by post-processing for the other MRT scans of the session, where subjects were instructed to stand still. The multi-slice EPI MRT sequence was then played at low SAR during 5 minutes to study temperature stability. Finally, this sequence was played at the maximal SAR allowed by the scanner to measure the temperature rise induced by RF power deposition. Two runs were performed on each subject, these scans being separated by ~10 minutes to allow for brain cooling. This 21-minute sequence was played at low SAR during the first minute and at maximal SAR for the next 20 minutes. Temperature change maps were computed without and with motion compensation, always with FS correction. The phase of the stability and 2n=16 heating scans was greatly affected by motion due to the relatively long acquisition times. To minimize data corruption from motion, only voxels for which the final time-course signals after motion compensation were not correlated to the scan motion regressors (with $R<0.5$) were kept in the analysis.

Results

Accuracy of the field sensor correction

In vitro measurements showed the high sensitivity of the phase (and thus temperature) to field perturbations likely originating both from the heating of the gradient and the shim, that resulted in a slow field drift, and from the field perturbations voluntarily induced by the movement of a

secondary phantom in the scanner tunnel (Figure 1b). Temperature change maps (Figure 1a, right) showed a hotspot located in the rear of the coil (Foot-Head direction), between the centre and the edge of the phantom, where maximum temperature rise reached approximately 0.8 °C for the image reconstructed with FS correction. Results at probe location (Figure 1b) showed that major field changes induced by the movement of the secondary phantom were captured by the field probes and corrected to a large extent, leading to a RMS error between MRT and optical probe measurements of 0.02 °C. Provided that the probe measurement is ground truth, this measure can be considered as an estimate of the method accuracy in this ideal motionless scenario. The uncorrected approach naturally failed to capture field perturbations.

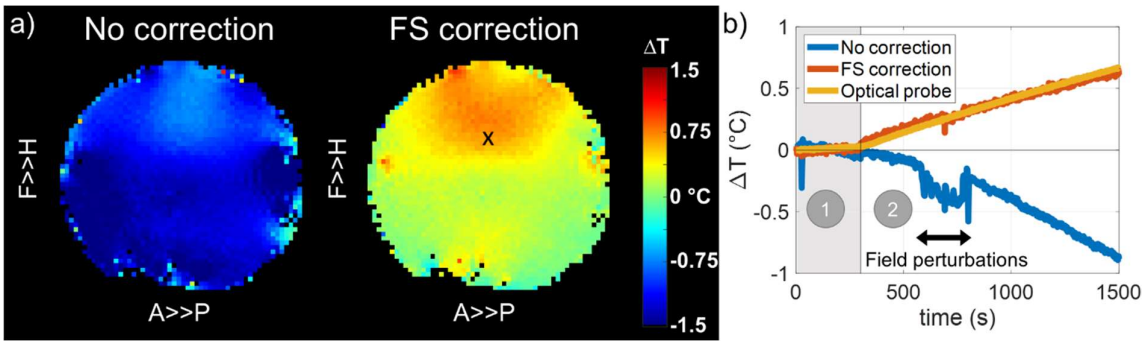

Figure 1: In vitro field sensor correction results. In vitro results for a 25-minute MRT scan performed on a 16-cm diameter spherical gel phantom with a pre-heating period of 5 minutes played at low SAR and followed by a heating period of 20 minutes played at maximal SAR. The field was deliberately disturbed between minutes 10 and 15 of the scan with movement of an additional phantom in the tunnel of the scanner. A fibre optical probe with 0.01°C sensitivity was used for ground truth measurements. a) Sagittal map of the temperature rise measured after 20 minutes of scanning at maximal SAR computed without correction and with field sensor (FS) correction. Distortions in EPI images resulted in flattening in the phase-encoding direction. b) Time course of temperature change measured in the phantom at probe location (represented by a black cross in Figure 1a). Zones 1 and 2 represent the pre-heating (low SAR) and heating (max SAR) periods, respectively.

Dictionary-based motion compensation scheme

An example of motion parameters estimated from the dictionary pre-scan of a volunteer is shown in Figure 2a. The influence of motion on the phase, and thus on temperature measurement, can be appreciated in Figure 2b where 1° rotations of the head already leads to 1 °C errors. Temperature change computed from motion-regressed phase resulted in a

much-reduced temporal standard deviation compared to the uncompensated approach in a large portion of the brain (Figures 2b and 2c), the periphery being still too sensitive to partial volume effects during image realignment.

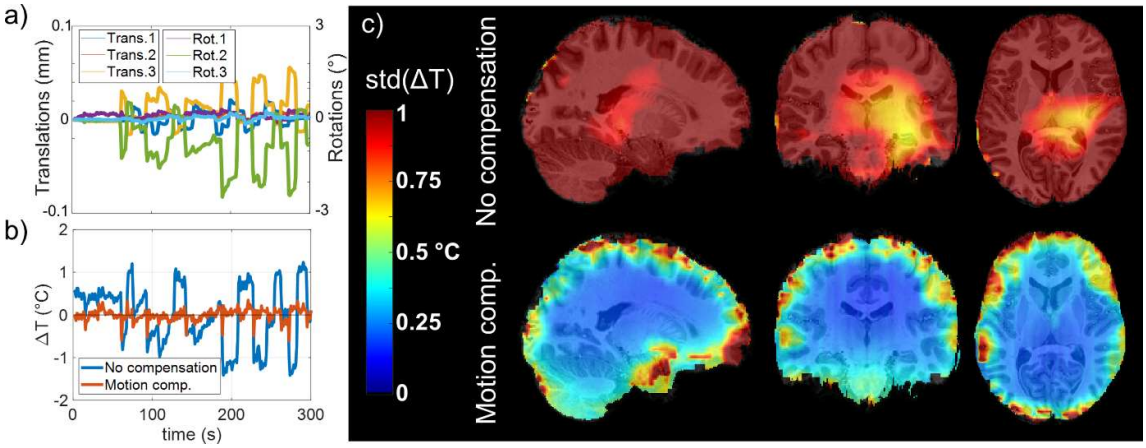

Figure 2: Pre-scan dictionary results for motion compensation. For each subject, the results of this scan were used to estimate the influence of low amplitude motion on the phase of the full-brain multi-slice MRT images. The subjects were instructed to explore different head positions during this 5-minute scan and to maintain each position for about 10 s. a) Example of the 6 motion parameters (3 rotation and 3 translations) estimated from the pre-scan of a subject. The influence of these parameters on the phase was voxel-wise regressed out. b) Temperature change time-course computed in a voxel of the same subject without and with motion compensation. c) Sagittal, coronal and axial maps of the temporal standard deviation measured on every subject without (top row) and with (bottom row) motion compensation, and averaged over the population after smoothing with a 9 mm kernel and normalisation to the MNI 3 mm brain template. This result is indicative of precision in extreme conditions.

Temperature stability when scanning at low SAR

Low-SAR scan results (Figure 3) show that a precision, quantified by the temporal standard deviation, of ~0.05°C could be reached on most parts of the brain with FS correction and motion compensation. As expected from this low-SAR scan, no temperature rise was observed over the brain.

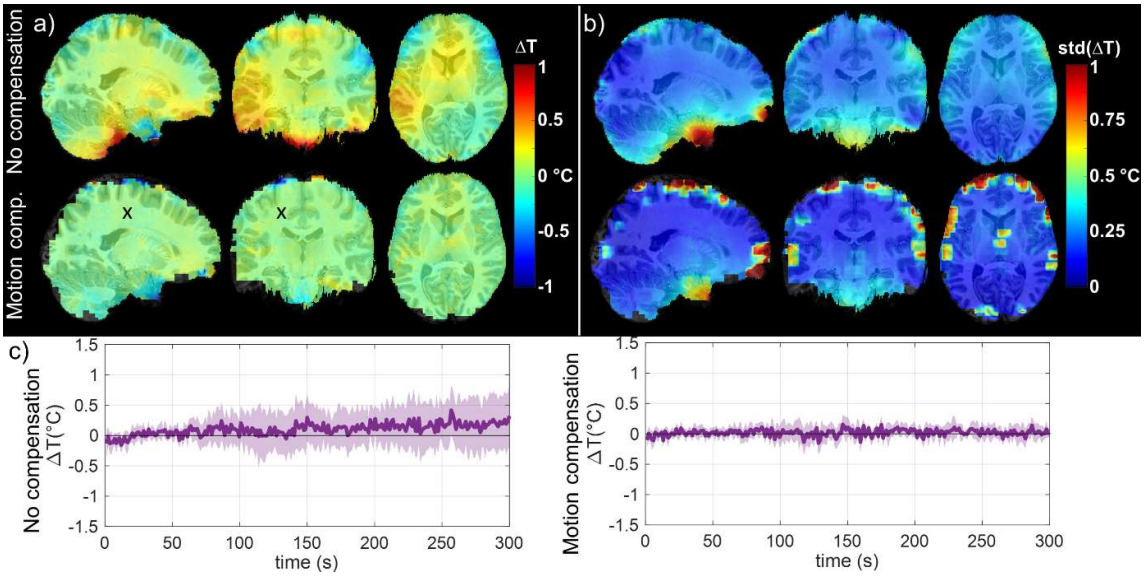

Figure 3: Results of the 5-minute MRT scan performed at low SAR level (n=8 runs). a) Median temperature change maps measured over the population for the low SAR scan without (top row) and with (bottom row) motion compensation. b) Corresponding temporal standard deviation maps averaged over the subjects. c) Time course of temperature change measured over the population (median value) in the voxel represented by a black cross in Figure 3a for every subject without (left) and with (right) motion compensation. This voxel is located 2 cm away from the midline. The standard deviation over subjects is represented in light colour.

Temperature rise when scanning at maximal SAR

Due to the long acquisition times of the maximal-SAR scans (21 minutes), temperature maps uncompensated for motion showed large variations across time and subjects (Figure 4), whereas the compensated approach was more robust. When averaged over the population, these scans showed only a slight temperature increase after 20 minutes of RF exposure (Figure 4a). The median temperature increase over the averaged brain was 0.1° (first quantile 0°C and third quantile 0.2°C) and it reached about only 0.2°C in the inner brain, where the SAR hotspot was expected (11), as represented by the black cross in Figure 4a. Small variations can be observed over the brain, but they are on the order of the standard deviation calculated across subjects. The temporal standard deviation was higher in the peripheral voxels of the brain. In most of the brain volume, otherwise the stability of the measurement indicated a temporal standard deviation of about 0.1 °C (Figure 4b). Regions where resonance

offsets are important (e.g. close to air cavities) also remained too sensitive with respect to motion. In the voxel represented by a black cross in Figures 3c and 4c, statistically brain heating resulting from the 20-min exposure at maximal SAR was higher that the temperature reached after 5-min scanning at low SAR (two-sided paired t-test with 8 degrees of freedom, p=0.04 and t=2.4).

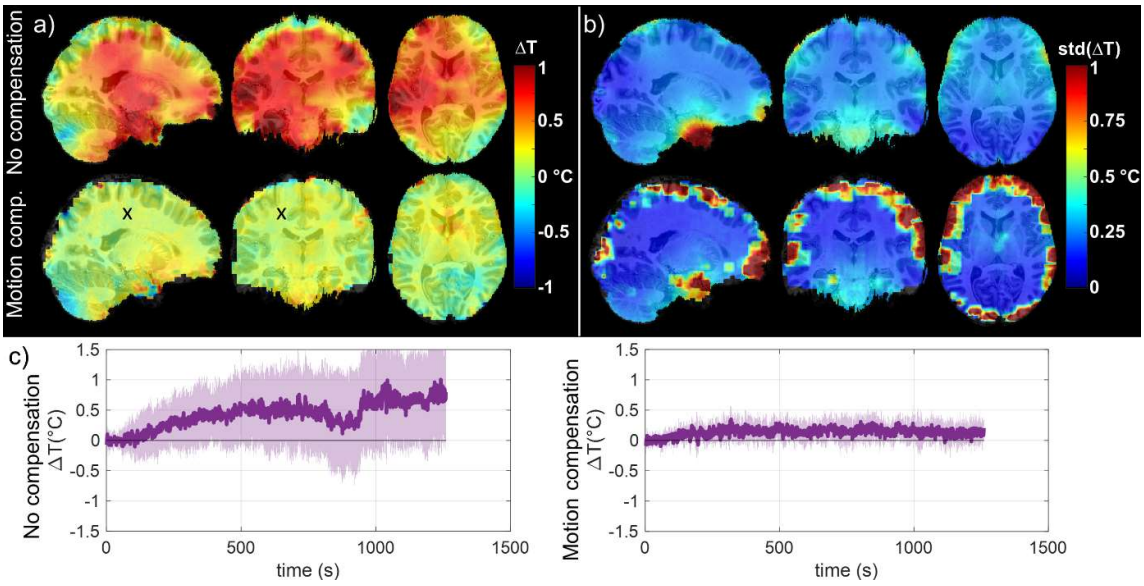

Figure 4: Results of the 20-minute MRT scans performed at maximal SAR (2n=16 runs). a) Median temperature change maps measured over the cohort after 20-minute exposure at maximal SAR. Temperature change maps were computed for every subject as the average over the last 5 minutes of the scan, without (top row) and with (bottom row) motion compensation, smoothing and normalisation to the MNI 3 mm brain template. b) Corresponding temporal standard deviation maps (averaged over the subjects and runs) as an indicative of temporal stability. c) Time course of temperature change measured over the population (median value) in the voxel represented by the black cross in Figure 4a, where the SAR hotspot is expected, without (left) and with (right) motion compensation. This voxel is located 2 cm away from the midline. The standard deviation across subjects is represented in light colour.

An example of temperature change with near full-brain coverage measured in one subject after FS correction and motion compensation is reported in Figure 5, showing small temperature changes in most of the inner brain volume. Voxels which temperature change remained correlated with motion, thus yielding positively or negatively large temperature excursions, were kept for illustration purposes. They were subsequently removed for the analysis in Figure 4.

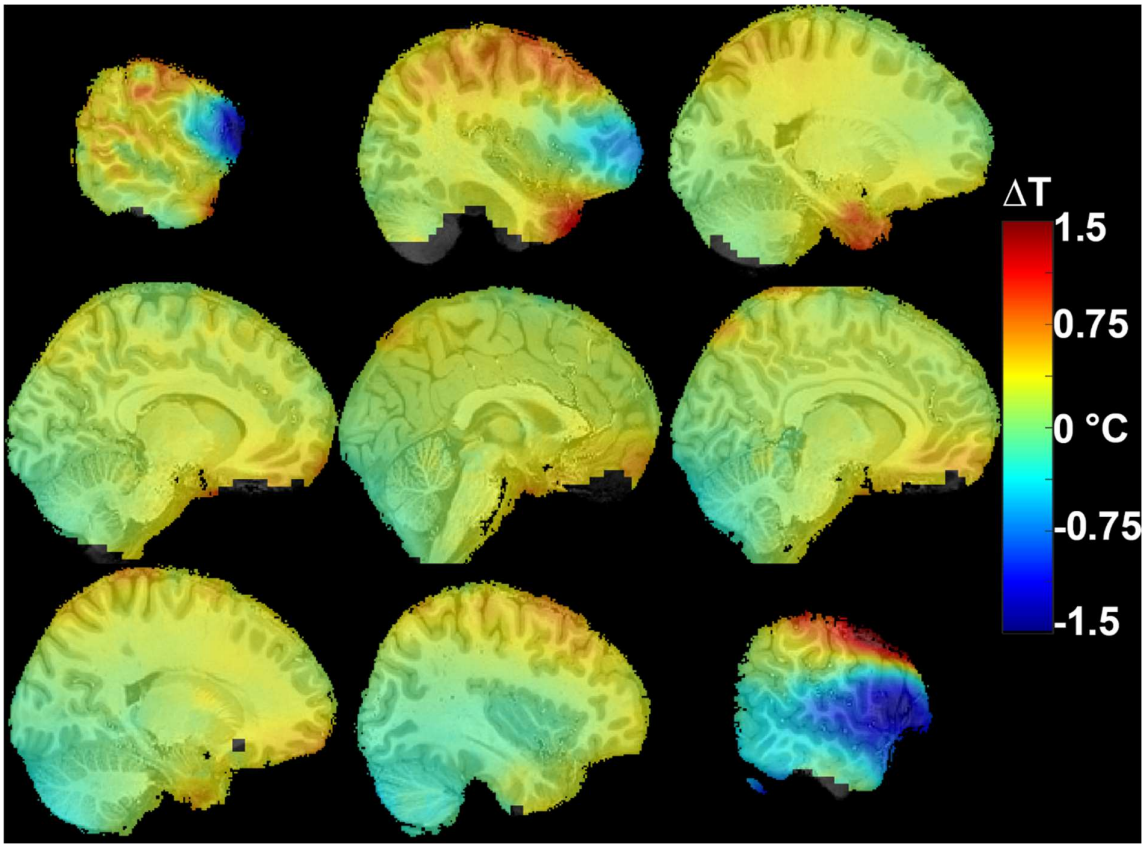

Figure 5: Example of temperature change measured on one subject of the cohort during the 20-minute scan at maximal SAR. Temperature change was computed with motion compensation but to preserve a full mask, no suppression of the voxels remaining correlated with motion parameters was performed. Those imperfectly corrected voxels led in this instance to illusory large temperature excursions (here blue and red areas), consistently with Figure 4.b where large uncertainties remained in the outer brain voxels.

Discussion

In the current study, PRFS temperature change measurement with correction of magnetic field fluctuations as measured with field sensors up to the second order of the spherical harmonics decomposition with an additional motion compensation step allowed reaching a precision of 0.05 °C on average over 8 subjects in most of the human brain with a full-brain multi-slice EPI sequence. The temperature rise induced by RF power deposition in the brain was measured for low and high SAR scans after phantom validation. Phantom experiments determined a 0.02 °C accuracy in a motionless scenario with the field sensor correction. The results obtained on the phantom showed the robustness of this methodology to accurately measure small temperature changes with field sensor correction despite the high sensitivity of the EPI

sequence to off-resonance effects, even in the presence of B_0 disturbances. These disturbances were induced by the movement of a second spherical phantom at the entrance of the scanner tunnel, which caused smooth field variations, as expected from breathing and limb motion. This appeared as a necessary first step to boost confidence in the in vivo results. In vivo, the phase remained highly sensitive to head motion even after field sensor correction as expected from simulations (17,27), resulting in temperature bias of several degrees. To retrieve the temperature rise induced by RF power deposition, a motion compensation step was thus found mandatory. The chosen approach was to characterize the influence of each motion parameter on the phase using a separate (dictionary) pre-scan. Despite all these precautions, temperature measurement in the voxels of the outer brain tended to have a higher uncertainty compared to the uncorrected approach, likely due to an improper motion compensation in these voxels and partial volume effects. For most voxels located in the inner brain volume, temperature precision reached 0.05 °C on average over the 8 subjects, as assessed from the temperature stability low SAR scan. Further improvement in temperature change sensitivity was limited by the cardiac pulsation, resulting in a periodic variation, and residual phase disturbance. Despite the absence of ground truth in vivo, the high intersubject reproducibility, the phantom results and the stability scans increased the confidence in the accuracy of the intensive SAR results.

After 20 minutes of scanning at the maximal SAR level allowed by the scanner in its normal mode of operation, RF-power deposition with the same RF coil induced a maximal temperature rise of approximately 0.8 °C in the phantom, with a heating pattern similar to the one reported in (11) for a head phantom (SAR hotspot at the top of the head), while brain temperature rose on average by 0.1 °C and no hotspot was observed. Interestingly, the difference between the low SAR and high SAR measurements was found statistically significant at the voxel where the SAR hotspot was expected. In the literature, only a limited number of studies have reported measurements of tissue temperatures in this regime, especially in the brain, continuously during RF exposure (15–17,33–35). A previous MRT experiment performed on the brain of an anaesthetised macaque with the same RF exposure scheme as the one used in the current study (20-minute scan acquired at maximal SAR) showed a slow rise in temperature that reached approximately 0.7 °C after 20 minutes (17). A direct measurement of RF-induced brain heating performed using fluoroptic probes in anaesthetised swine showed a continuous temperature increase that could reach more than 1 °C (15), although head and body coils certainly can lead to different exposures. The comparison between these animal and the current human studies is however not straightforward due to anatomical differences between species and the use of anaesthetic agents on the animals that can affect thermoregulation. For instance, a study of RF exposure performed on anaesthetised and non-anaesthetised rats

has shown that when exposed at the same SAR level, non-anaesthetised rats were able to maintain their body temperature while the anaesthetised ones had an increased body temperature eventually leading to death (36). A study performed on the human calf, a poorly perfused muscle, also reported a continuous temperature rise that reached several degrees (35). Interestingly, a study using an MR spectroscopy-based thermometry approach showed cerebral temperature increases in humans of 0.4 °C when drinking hot water (37). Our results would thus indicate that a 20 min scan at the current maximal SAR limit, including a safety factor, is more benign for the brain from the thermal point of view than hot water ingestion. International safety guidelines indicate that the absolute temperature in the brain should not exceed 39 °C during the MR exam. The proposed method characterizes temperature changes and therefore cannot lead to a strict verification of these guidelines unless the basal temperature with its intrinsic gradients are known beforehand (4,6,38).

Phantom experiments performed in this study and elsewhere (11,17) as well as animal experiments (17) confirmed in this setup non-negligible power depositions compared to IEC guidelines. Without heat diffusion and perfusion, a linear increase of ~0.3 °C/(W/kg) would be expected for a 20 minutes RF exposure, while full numerical studies based on PBE (19,29) predicted maximum local temperature rises in the brain of 0.5-1 °C for other volume coils but for comparable head-averaged SAR. Our results thus would suggest more heat dissipation in awake humans than anticipated.

A limit of this study is that the temperature measurement was limited to the central part of the brain, whereas its periphery could not be accurately compensated for motion. The temperature rise occurring in other tissues (e.g. skin, eyes), which are also of interest for RF safety, could not be measured with this protocol. However, these results are encouraging since the SAR hotspot is expected to arise for this setup at the top of the brain according to simulations and head phantom measurements (11), where temperature rise in the current study was measured in vivo on the order of 0.2 °C when exposed at maximal SAR levels. Interestingly also, basal temperatures are expected to be lower than 37 °C in the skin area (39) so that larger RF-induced temperature rises could be tolerated there. Ideally, further measurements would be needed to validate this assessment. Another limit is that temperature variation estimates are proportional to the PRFS coefficient, taken here as -0.01 ppm/°C by default, as in most studies. Considering the range of -0.007 to -0.013 ppm/°C reported in the literature (40), this could constitute a bias and affect our temperature results by ± 30%. Other sources of potential bias include imperfect motion estimate and compensation. These difficulties could be potentially overcome by using spectroscopy-based MRT approaches (41,42). While this method could be used to measure temperature in the brain during hour-long MR exams (23,38), it would not allow a sufficient spatiotemporal resolution to sample the brain thermal response to RF

exposure as aimed here. Another perspective of this study is to explore RF power deposition resulting from mobile phone wave exposure in vivo, inside an MRI scanner, where SAR also has remained the gold standard for simplicity.

In conclusion, this study introduced an MR-thermometry based methodology that allowed measuring temperature increases with a precision of 0.05 °C non-invasively in the inner brain. When applied to a scan performed at maximal SAR in normal RF exposure conditions, a temperature rise of 0-0.2 °C was measured, a result significantly different from the low SAR scan. The data acquired represent the first experimental evidence suggesting that there could be leeway to gain performance in brain MR exams and that SAR thresholds and safety margins could be potentially revisited.

ACKNOWLEDGEMENTS

This work received financial support from Leducq Foundation (large equipment Equipement de Recherche et Plateformes Technologiques program, NEUROVASC7T project), and from the European Union Horizon 2020 Research and Innovation program under grant agreements no. 736937 (M-Cube) and 885876 (AROMA). We also thank K. Pruessmann, D. Brunner, C. Barmet and M. Kozlov for valuable discussions.

References

1. Ross EZ, Cotter JD, Wilson L, Fan J-L, Lucas SJE, Ainslie PN. Cerebrovascular and corticomotor function during progressive passive hyperthermia in humans. Journal of Applied Physiology 2012;112:748–758 doi: 10.1152/japplphysiol.00988.2011.

2. Bazille C, Megarbane B, Bensimhon D, et al. Brain Damage After Heat Stroke: Journal of Neuropathology and Experimental Neurology 2005;64:970–975 doi: 10.1097/01.jnen.0000186924.88333.0d.

3. Shih C-J, Lin M-T, Tsai S-H. Experimental study on the pathogenesis of heat stroke. Journal of Neurosurgery 1984;60:1246–1252 doi: 10.3171/jns.1984.60.6.1246.

4. Wang H, Wang B, Normoyle KP, et al. Brain temperature and its fundamental properties: a review for clinical neuroscientists. Front Neurosci 2014;8:307 doi: 10.3389/fnins.2014.00307.

5. Dehkharghani XS, Fleischer XCC, Qiu XD, Yepes XM, Tong XF. Cerebral Temperature Dysregulation: MR Thermographic Monitoring in a Nonhuman Primate Study of Acute Ischemic Stroke. :9.

6. Campos F, Blanco M, Barral D, Agulla J, Ramos-Cabrer P, Castillo J. Influence of temperature on ischemic brain: Basic and clinical principles. Neurochemistry International 2012;60:495–505 doi: 10.1016/j.neuint.2012.02.003.

7. Marshall I, Karaszewski B, Wardlaw JM, et al. Measurement of regional brain temperature using proton spectroscopic imaging: validation and application to acute ischemic stroke. Magnetic Resonance Imaging 2006:8.

8. IEC. Medical electrical equipment-Part 2-33: Particular requirements for the basic safety and essential performance of magnetic resonance equipment for medical diagnosis. 2015;Edition 3.2.

9. Rieke V, Instrella R, Rosenberg J, et al. Comparison of temperature processing methods for monitoring focused ultrasound ablation in the brain. Journal of Magnetic Resonance Imaging 2013;38:1462–1471 doi: 10.1002/jmri.24117.

10. Quesson B, Zwart JA de, Moonen CTW. Magnetic resonance temperature imaging for guidance of thermotherapy. Journal of Magnetic Resonance Imaging 2000;12:525–533 doi: 10.1002/1522-2586.

11. Insua IG, Gumbrecht R, Wicklow K, Polimeni JR. Determination of local SAR through MR Thermometry at 7T. In Proceedings of the 27th Annual Meeting of ISMRM, Montreal 2019:abstract 4182.

12. Pennes HH. Analysis of Tissue and Arterial Blood Temperatures in the Resting Human Forearm. Journal of Applied Physiology 1948;1:93–122 doi: 10.1152/jappl.1948.1.2.93.

13. Kotte A, Leeuwen G van, Bree J de, Koijk J van der, Crezee H, Lagendijk J. A description of discrete vessel segments in thermal modelling of tissues. Phys. Med. Biol. 1996;41:865–884 doi: 10.1088/0031-9155/41/5/004.

14. Shrivastava D, Vaughan JT. A Generic Bioheat Transfer Thermal Model for a Perfused Tissue. Journal of Biomechanical Engineering 2009;131:074506 doi: 10.1115/1.3127260.

15. Shrivastava D, Hanson T, Kulesa J, Tian J, Adriany G, Vaughan JT. Radiofrequency heating in porcine models with a “large” 32 cm internal diameter, 7 T (296 MHz) head coil. Magnetic Resonance in Medicine 2011;66:255–263 doi: 10.1002/mrm.22790.

16. Boulant N, Bottlaender M, Uhrig L, et al. FID navigator-based MR thermometry method to monitor small temperature changes in the brain of ventilated animals. NMR Biomed. 2014 doi: 10.1002/nbm.3232.

17. Le Ster C, Mauconduit F, Mirkes C, et al. RF heating measurement using MR thermometry and field monitoring: Methodological considerations and first in vivo results. Magnetic Resonance in Medicine 2021;85:1282–1293 doi: https://doi.org/10.1002/mrm.28501.

18. Hunter WS, Holmes KR, Elizondo RS. Thermal balance in ketamine-anesthetized rhesus monkey Macaca mulatta. American Journal of Physiology-Regulatory, Integrative and Comparative Physiology 1981;241:R301–R306 doi: 10.1152/ajpregu.1981.241.5.R301.

19. Collins CM, Liu W, Wang J, et al. Temperature and SAR calculations for a human head within volume and surface coils at 64 and 300 MHz. Journal of Magnetic Resonance Imaging 2004;19:650–656 doi: 10.1002/jmri.20041.

20. Lier ALHMW van, Kotte ANTJ, Raaymakers BW, Lagendijk JJW, Berg CAT van den. Radiofrequency heating induced by 7T head MRI: Thermal assessment using discrete vasculature or pennes’ bioheat equation. Journal of Magnetic Resonance Imaging 2012;35:795–803 doi: https://doi.org/10.1002/jmri.22878.

21. Murbach M, Neufeld E, Cabot E, et al. Virtual population-based assessment of the impact of 3 Tesla radiofrequency shimming and thermoregulation on safety and B1+ uniformity. Magnetic Resonance in Medicine 2016;76:986–997 doi: 10.1002/mrm.25986.

22. Rieke V, Pauly KB. MR thermometry. Journal of Magnetic Resonance Imaging 2008;27:376–390 doi: 10.1002/jmri.21265.

23. Fleischer CC, Wu J, Qiu D, Park S-E, Nahab F, Dehkharghani S. The Brain Thermal Response as a Potential Neuroimaging Biomarker of Cerebrovascular Impairment. AJNR Am J Neuroradiol 2017;38:2044–2051 doi: 10.3174/ajnr.A5380.

24. Hindman JC. Proton Resonance Shift of Water in the Gas and Liquid States. The Journal of Chemical Physics 1966;44:4582–4592 doi: 10.1063/1.1726676.

25. Wlodarczyk W, Hentschel M, Wust P, et al. Comparison of four magnetic resonance methods for mapping small temperature changes. Phys. Med. Biol. 1999;44:607–624 doi: 10.1088/0031-9155/44/2/022.

26. Peters RTD, Hinks RS, Henkelman RM. Ex vivo tissue-type independence in proton-resonance frequency shift MR thermometry. Magnetic Resonance in Medicine 1998;40:454–459 doi: 10.1002/mrm.1910400316.

27. Liu J, de Zwart JA, van Gelderen P, Murphy-Boesch J, Duyn JH. Effect of head motion on MRI B0 field distribution: Liu et al. Magnetic Resonance in Medicine 2018;80:2538–2548 doi: 10.1002/mrm.27339.

28. Barmet C, Zanche ND, Pruessmann KP. Spatiotemporal magnetic field monitoring for MR. Magnetic Resonance in Medicine 2008;60:187–197 doi: 10.1002/mrm.21603.

29. Wang Z, Lin JC, Mao W, Liu W, Smith MB, Collins CM. SAR and temperature: Simulations and comparison to regulatory limits for MRI. Journal of Magnetic Resonance Imaging 2007;26:437–441 doi: https://doi.org/10.1002/jmri.20977.

30. Simonis FFJ, Petersen ET, Bartels LW, Lagendijk JJW, Berg CAT van den. Compensating for magnetic field inhomogeneity in multigradient-echo-based MR thermometry. Magnetic Resonance in Medicine 2015;73:1184–1189 doi: https://doi.org/10.1002/mrm.25207.

31. Ehses P, Fidler F, Nordbeck P, et al. MRI thermometry: Fast mapping of RF-induced heating along conductive wires. Magnetic Resonance in Medicine 2008;60:457–461 doi: 10.1002/mrm.21417.

32. Wilm BJ, Barmet C, Pavan M, Pruessmann KP. Higher order reconstruction for MRI in the presence of spatiotemporal field perturbations. Magnetic Resonance in Medicine 2011;65:1690–1701 doi: 10.1002/mrm.22767.

33. Eryaman Y, Lagore RL, Ertürk MA, et al. Radiofrequency heating studies on anesthetized swine using fractionated dipole antennas at 10.5 T. Magnetic Resonance in Medicine 2018;79:479–488 doi: 10.1002/mrm.26688.

34. Nadobny J, Klopfleisch R, Brinker G, Stoltenburg-Didinger G. Experimental investigation and histopathological identification of acute thermal damage in skeletal porcine muscle in relation to whole-body SAR, maximum temperature, and CEM43 °C due to RF irradiation in an MR body coil of birdcage type at 123 MHz. International Journal of Hyperthermia 2015;31:409–420 doi: 10.3109/02656736.2015.1007537.

35. Simonis FFJ, Raaijmakers AJE, Lagendijk JJW, van den Berg CAT. Validating subject-specific RF and thermal simulations in the calf muscle using MR-based temperature measurements: Validating RF and Thermal Simulations with MRI Measurements. Magn. Reson. Med. 2017;77:1691–1700 doi: 10.1002/mrm.26244.

36. Kim HS, Lee YH, Choi H, et al. Effect of Exposure to a Radiofrequency Electromagnetic Field on Body Temperature in Anesthetized and Non-Anesthetized Rats. Bioelectromagnetics 2020;41:104–112 doi: 10.1002/bem.22236.

37. Yoshioka Y, Oikawa H, Kanbara Y, et al. Physiological brain temperature change is detectable by MRS. In Proceedings of the 19th Annual Meeting of ISMRM, Montreal 2011:Abstract 1443.

38. Dehkharghani S, Fleischer CC, Qiu D, Yepes M, Tong F. Cerebral Temperature Dysregulation: MR Thermographic Monitoring in a Nonhuman Primate Study of Acute Ischemic Stroke. AJNR Am J Neuroradiol 2017;38:712–720 doi: 10.3174/ajnr.A5059.

39. Massire A, Cloos MA, Luong M, et al. Thermal simulations in the human head for high field MRI using parallel transmission. Journal of Magnetic Resonance Imaging 2012;35:1312–1321 doi: 10.1002/jmri.23542.

40. Kuroda K. Non-invasive MR thermography using the water proton chemical shift. International Journal of Hyperthermia 2005;21:547–560 doi: 10.1080/02656730500204495.

41. Cady EB, D'Souza PC, Penrice J, Lorek A. The Estimation of Local Brain Temperature by in Vivo 1H Magnetic Resonance Spectroscopy. Magnetic Resonance in Medicine 1995;33:862–867 doi: 10.1002/mrm.1910330620.

42. Corbett RJT, Laptook AR, Tollefsbol G, Kim B. Validation of a Noninvasive Method to Measure Brain Temperature In Vivo Using 1H NMR Spectroscopy. Journal of Neurochemistry 1995;64:1224–1230 doi: 10.1046/j.1471-4159.1995.64031224.x.